Repeating earthquakes in the Yellowstone volcanic field: Implications for rupture dynamics, ground deformation, and migration in earthquake swarms

Frédérick Massin *, Jamie Farrell, Robert B. Smith

Department of Geology and Geophysics, Salt Lake City, UT, 84112, USA

ARTICLE INFO

ABSTRACT

We evaluated properties of Yellowstone earthquake swarms employing waveform multiplet analysis. Thirty-seven percent of the earthquakes in the Yellowstone caldera occur in multiplets and generally intensify in areas undergoing crustal subsidence. Outside the caldera, in the Hedgen Lake tectonic area, the clustering rate is higher, up to 75%. The Yellowstone seismicity follows a succession of two phases of earthquake sequence. The first phase is defined between swarms. It is characterized by a decay of clustering rate and by foreshock–aftershock sequences. The second phase is confined to swarms and is characterized by an increase in clustering rate, and dominant aftershock sequences. This phase reflects tectonic swarms that occur on short segments of optimally oriented faults. For example, the largest recorded swarm in Yellowstone occurred in autumn 1985 on the northwest side of the Yellowstone Plateau which was initiated as a tectonic source sequence. Fitting experimental dependence of fluid injection with intrusion migration suggests that the 1985 swarm involved, after 10 days, hydrothermal fluids flowing outward from the caldera. The 2008–2009 Yellowstone Lake swarm exhibited a high migration rate of 1 km/day, a decrease in clustering rate without a main-shock, and appears to be associated with magma injection of 1 to 5 m^3/s in a succession of migrating magma fronts that incrementally solidify and fracture at its brittle edges. The 2010 Madison Plateau earthquake swarm on the west side of the caldera initiated as a tectonic sequence but the expansion of the swarm front was associated with hydrothermal fluid migration.

1. Introduction

Earthquake swarms consist of a series of earthquakes closely clustered in space and time without a clear main-shock (Mogi, 1963; Sykes, 1970). Magmatic intrusion can occur coincidently with earthquake swarms in volcanic settings, raising the question of how to distinguish between earthquakes driven by magmatic and tectonic processes and homogeneity of the associated stress field (Bergman and Solomon, 1990; Ruppert et al., 2011). Hill (1977) for example, noted that active volcanic systems commonly experience swarms as a main mode of seismic energy release. However earthquake swarms are not exclusively associated with volcanism (Benoit and McNutt, 1996). Identifying the statistical and quantitative properties of earthquake swarms aid in distinguishing their driving processes. A key characteristic of some Yellowstone earthquake swarms is the migrating front of the hypocenter pattern. Non-migrating swarms are often associated with the release of tectonic stress through an earthquake sequence in which each event participates in the triggering of the next, whereas spatial migration of swarm fronts can best be modeled as fluid related diffusion, i.e., pressurized fluids that triggered incipient fractures and related earthquakes in their migration path.

Tectonic earthquake swarms occur in a variety of fault conditions including regional extensional stress regimes (for example along mid-ocean ridges, Bergman and Solomon, 1990), strike-slip systems (for example on the San Andreas fault, McNally et al., 1978) and subduction zones (swarms associated with the circum-Pacific subduction zone are detailed in Holtkamp and Brudzinski, 2011). While some tectonic swarms progressively end with little consequence (e.g. no large main-shock), others can become foreshock sequences to larger main-shocks and can be interpreted, in retrospect, as precursors (Evison and Rhoades, 1998).

Migrating swarms may result from a temporal stress field perturbation due to a mobile component of crustal fluids (Rubin, 1995) or a mobile and concentrated stress perturbation (Mogi, 1963). Migration of hydrothermal fluid also has been shown to induce migrating earthquake swarms by increasing pore fluid pressure and reduction of the effective normal stress (Fournier, 1999). Magma transport, whether breaching the surface or not, often triggers migrating earthquake swarms by failure at the dike tip or failure of the magma reservoir wall (Hill, 1977; Rubin, 1995; Ukase and Tsukahara, 1996; Roman and Cashman, 2006). The occurrence of earthquake swarms and the variety of triggering processes can complicate both volcano and earthquake hazard assessment. The Yellowstone volcanic field and related areas of strong seismicity offer the opportunity to study both tectonic and magmatic swarms requiring a modern seismic and GPS network such as in Yellowstone.

* Corresponding author. Tel.: +1 801 581 7856; fax: +1 801 581 7065.
  E-mail address: frederick.massin@univ-ag.fr (F. Massin).

1.1. Yellowstone earthquake swarms

The Quaternary rhyolite plateau of Yellowstone National Park (hereafter, "Yellowstone") dominates the geologic setting (Fig. 1). It is the result of bimodal basaltic–rhyolitic volcanism in the lithospheric extensional stress regime of the Basin-Range province (summarized by Smith et al., 2009). It has been shown from seismic tomography that an upper-mantle plume feeds Yellowstone volcanism (Waite et al., 2006; Smith et al., 2009; Obrebski et al., 2010). The plume feeds basaltic fluid into the lower crust and melts the mid and upper crust to form a rhyolitic/basaltic magma reservoir of up to 15% melt (Husen et al., 2004a, 2004b; Smith et al., 2009) underlying the 0.64 Ma Yellowstone caldera (see Fig. 1, and Christiansen, 2001) at depths of 5 to 15 km.

Crustal extension and the crustal magma system in Yellowstone are characterized by the highest conductive heat-flux of the western U.S., ~2 W/m^2 (DeNosaquo et al., 2009; Smith et al., 2009). Also, Yellowstone seismicity is characterized by the highest rate of earthquake activity of the Intermountain Seismic Belt (0.12 eq/km^2/yr) compared to the central Intermountain Seismic Belt (0.03 eq/km^2/yr, Smith et al., 2009). Kinematically, the Yellowtone caldera has undergone multiple cycles of crustal subsidence and uplift at the decade-scale at rates as high as 7 cm/yr (Chang et al., 2007; Puskas et al., 2007; Chang et al., 2010).

Volcano and earthquake hazards (Christiansen et al., 2007), underscored by the deadly Mw7.3, 1959 Hebgen Lake earthquake, on the west side of the Yellowstone Plateau (Chang and Smith, 2002; Pickering-White et al., 2009; Smith et al., 2009) justify the operation of a modern seismic and GPS monitoring network in Yellowstone, operating since 1972, from which we derived the data used in this study.

Yellowstone experiences a few hundred to 3000 earthquakes per year, 100 to 150 earthquakes per year being over the maximum magnitude of completeness, estimated to Mc = 1.5 (Farrell et al., 2009). On average, ~44% of Yellowstone earthquakes occur in swarms, releasing ~40% of the total seismic moment (Farrell et al., 2009). Between 1985 and 2011, there has been 90 independent earthquake swarms (Farrell et al., 2009).

For this paper we will examine three of the most important Yellowstone earthquake swarms with well-defined migrating hypocenter fronts. These include (1) the autumn 1985 northwest Yellowstone caldera earthquake swarm (hereafter, AYES, Waite and Smith, 2002), (2) the 2008–2009 Yellowstone Lake earthquake swarm (YLES) documented by Farrell et al. (2010a, 2010b) and (3) the 2010 Madison Plateau earthquake swarm (MPES) documented by Farrell et al. (2010a, 2010b) and Shelly et al. (2012). The relationship between these swarms and the magmatic fluid–rock interactions however is problematic. Moreover better hazard assessment of Yellowstone relies on the ability to discriminate between tectonic, magmatic, and swarms triggered by fluid pressure variations, a key objective of this paper.

1.2. Earthquake swarm characterization approach

We employed multiplet analysis to infer time–spatial properties of Yellowstone seismicity that contributes to the understanding of source characterization and process of swarm generation. In this study, we use the term "multiplet" to define a group of earthquakes produced by the re-activation of a self-similar seismic source sharing a common hypocenter location, and characterized by similar body-wave waveforms (Geller and Mueller, 1980; Poupinet et al., 1984; Fremont and Malone,
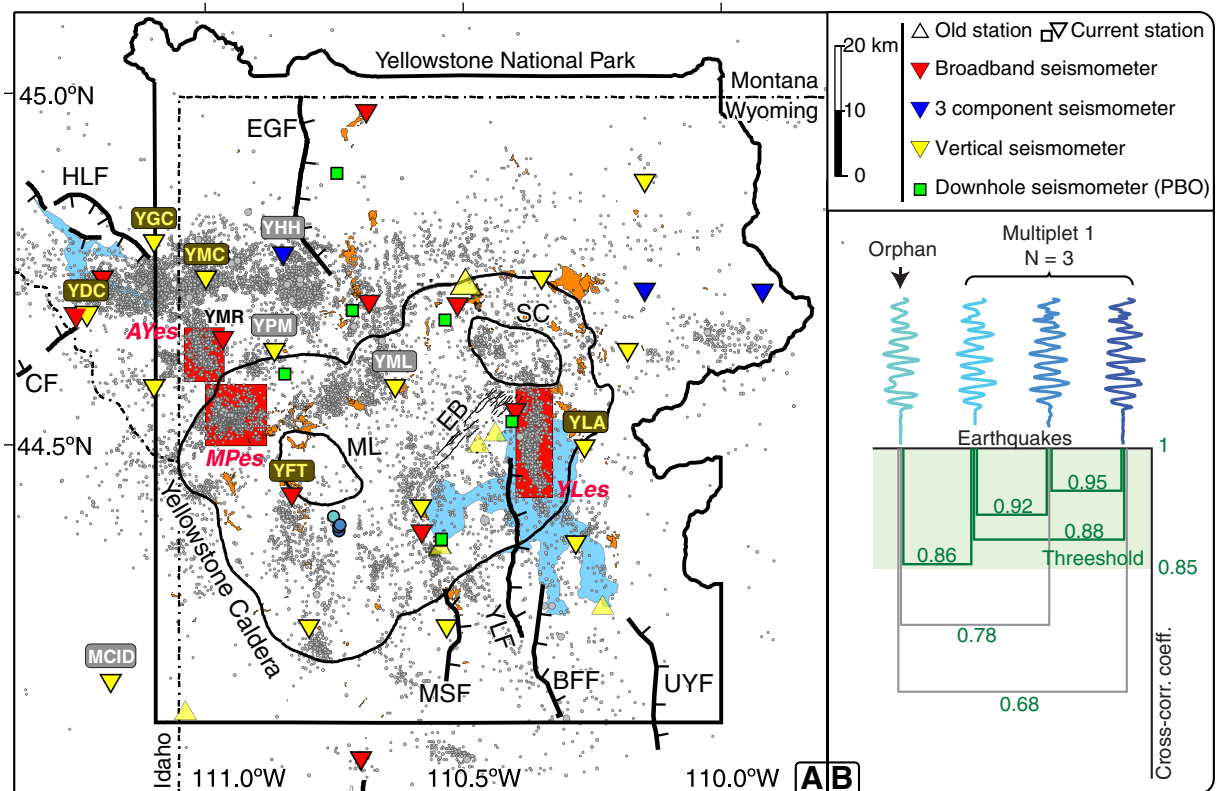

Fig. 1. Map of Yellowstone showing the seismic network stations and earthquakes. Faults are abbreviated as HLF: Hebgen Lake fault; CF: Centennial fault; EGF: East Gallatin fault; MSF: Mt. Sheridan fault; YLF: Yellowstone Lake fault; BFF: Buffalo Fork fault; UYF: Upper Yellowstone Valley fault; ML: Mallard Lake resurgent dome; SC: Sour Creek resurgent dome; EB: Elephant Back fault system). A, gray dots: 33054 earthquake epicenters from 1981 to 2010. A, triangles and squares: seismic stations (see legend). Gray labels: seismic stations used for waveform clustering from 1992 to 2010. Brown labels: seismic stations used for waveform clustering from 1984 to 2010. The chosen set of seismometers provided at least two P-wave picks for every earthquake. B: clustering scheme. Multiplets are made of doublets, which are pairs of earthquakes with a waveform cross correlation coefficients over 0.85 on two stations.

1987). We employ the following terms for details of the multiplet definition:

(1) "orphan earthquakes" for earthquakes that are not part of an identified multiplet,
(2) "repeating earthquakes" for all events being part of any multiplet at a given time or area.
(3) "multiplet earthquakes" to refer to events from one specific multiplet,
(4) dual multiplet earthquakes make up a "doublet",
(5) "total earthquakes" for all earthquakes not of the orphan or repeating earthquakes.

Multiplets are generally used to investigate the main seismogenic structures (Got and Okubo, 2003; Massin et al., 2011) whereas our principal objective was to evaluate the multiplet-rupture modes in Yellowstone earthquakes using multiplet seismic cycle, ground deformation, and swarm modeling of the migration of hypothetic magma-related fluids.

2. Multiplet earthquake analysis

Here we define the process used to retrieve multiplets, that is similar to that by Got et al. (1994), Rowe et al. (2002, 2004), Thelen et al. (2008), and Massin et al. (2011). The first step is populating a working Yellowstone earthquake waveform catalog with data from the University of Utah Seismograph Stations (UUSS).

2.1. Yellowstone seismic network and data

The UUSS operates the Yellowstone seismic network (Fig. 1A) that has consisted of up to forty-seven seismic stations. We use the seismic analyst's manually picked and reviewed P- and S-wave arrivals and the earthquake waveforms produced by the UUSS. The earthquake listing that we used contains 33,054 earthquakes that have been located by the UUSS analysts between 1984 and June 2010 using a one-dimensional velocity model (Fig. 1A). It is important to note on Fig. 1A that the network density was greatly improved between 1992 and 1994 with the addition of five vertical short period and two three-component short-period seismometers. In addition, a major upgrade to the network was made from 2009 to 2011 from the ARRA (American Recovery and Reinvestment Act) by USGS and NPS funding that included installation of two vertical short-period, seven three-component short-period, 11 broadband seismometers and seven accelerometers whose data were invaluable to this study. Farrell et al. (2009) determined that the threshold of minimum magnitude of completeness for the Yellowstone network is 1.5 before 1994 and 1.2 after 1994. The long-term network operation allows for the analysis of multiplets that spanned the entire 1984–2010 time period used in this study.

Because of the temporal evolution of the seismic network, two station groups were chosen to investigate earthquake similarities. The data from stations YLA, YFT, YMC, YGC, and YDC (brown labels on Fig. 1A) provided at least two body-wave waveforms for all the 1984–2010 earthquakes. To enhance our multiplet catalog, we also employed a second set of stations (YHH, YMP, MCID, YML and YLA, gray labels on Fig. 1A) providing a minimum of two body wave waveforms for all of the earthquakes between 1992 and 2010. The two station groups are used for multiplet analysis in two steps described below.

2.2. Earthquake clustering

As detailed in this section, we employed an improved version of the Massin et al. (2011) clustering algorithm that facilitates the updating of the multiplet catalog with new data. First we identified multiplets from 1992 to 2010 from the first station group. The multiplet catalog was then updated using the 1984–1992 data. The earthquake multiplets were identified by grouping earthquakes that were similar based on a chosen criterion of P and S waveforms similarity, a process named clustering by Everitt (1974). Fig. 1B represents our clustering scheme with an example of an earthquake dataset. To have both the P- and the S-waves from a single event, we extracted five-second long waveforms from the vertical component of the two station sets. Each independent waveform starts a half second before the P-wave arrival and finishes 4.5 s later.

In Fig. 1B, the clustering criterion defines two earthquakes as a doublet if the cross-correlation coefficient between their waveforms is 0.85 or higher on at least two stations (green links on Fig. 1B). The dominant frequencies of the Yellowstone earthquake data used in the study are from 0.8 to ~8 Hz. To reduce noise effects and magnitude dependencies, the waveform data are filtered between 1 and 12 Hz to produce a uniform data set. The average dominant frequency is 3.1 Hz and corresponds to a theoretical doublet separation of 500 m (Geller and Mueller, 1980). In our dataset, earthquake pairs separated by 500 m, taking into account location errors, reach cross correlation coefficients over 0.8. Further analysis of correlation coefficients shows that a 0.85 threshold selects the most significant higher correlations, i.e., less than 0.5% of all possible waveform pairs in our dataset. We thus choose a cross-correlation value of 0.85 as a threshold to select all the earthquake pairs within the range of separation of theoretical 3.1 Hz doublets and showing significant high cross-correlation coefficients. The window length and the correlation threshold were chosen for waveform similarity beyond the 5 s window, along the coda waves, as in Fig. 2A.

We retrieve discreetly identified multiplets by merging all the doublets of each earthquake, starting with the earthquake with the most doublets. We then update the multiplet list with the older data, only the multiplets highest magnitude clustered waveforms and orphan waveforms are cross-correlated with the 1984–1992 waveforms. Fig. 2A shows an example of a multiplet waveform. This multiplet shows nearly identical body, surface, and coda waveforms from 1994 to 2010 along 130 earthquakes. As with the others, this multiplet set consists of repeating earthquakes occurring on the same fault plane in a medium of stable physical properties. The clustering results are examined in their chronology, through clustering rate and seismic cycle.

3. Temporal evolution of multiplets

3.1. Multiplets chronology during swarm nucleation

Between 1984 and 2010, 15,874 of the 33,054 earthquakes (48%) have repeating waveforms. The simplified dendrogram in Fig. 2B represents earthquake doublets chronologically during the 1984–2010 time period. Each doublet is depicted by two green dots, at the time of the multiplet earthquakes, linked by a horizontal gray line. Each horizontal group of doublets represents a multiplet. Multiplets are ordered by origin time of their first earthquake. The swarm time periods originally designated by Farrell et al. (2009) are represented by light brown lines.

The general tendency of multiplet chronology (Fig. 2B) is for a succession of two phases: 1) one at a constant rate of multiplets with various lifetimes between swarms; and 2) one with an exponential increase of day-long multiplets during swarms. As explained in Section 2, the increase in station density results in lowering the magnitude of completeness of the Yellowstone earthquake catalog after 1994. Considering only the 400 to 550 total earthquakes per year over the magnitude of completeness would not allow a satisfying temporal analysis. Consequently, for statistical analysis of our clustering result we used only the multiplets from the period 1994 to 2010.
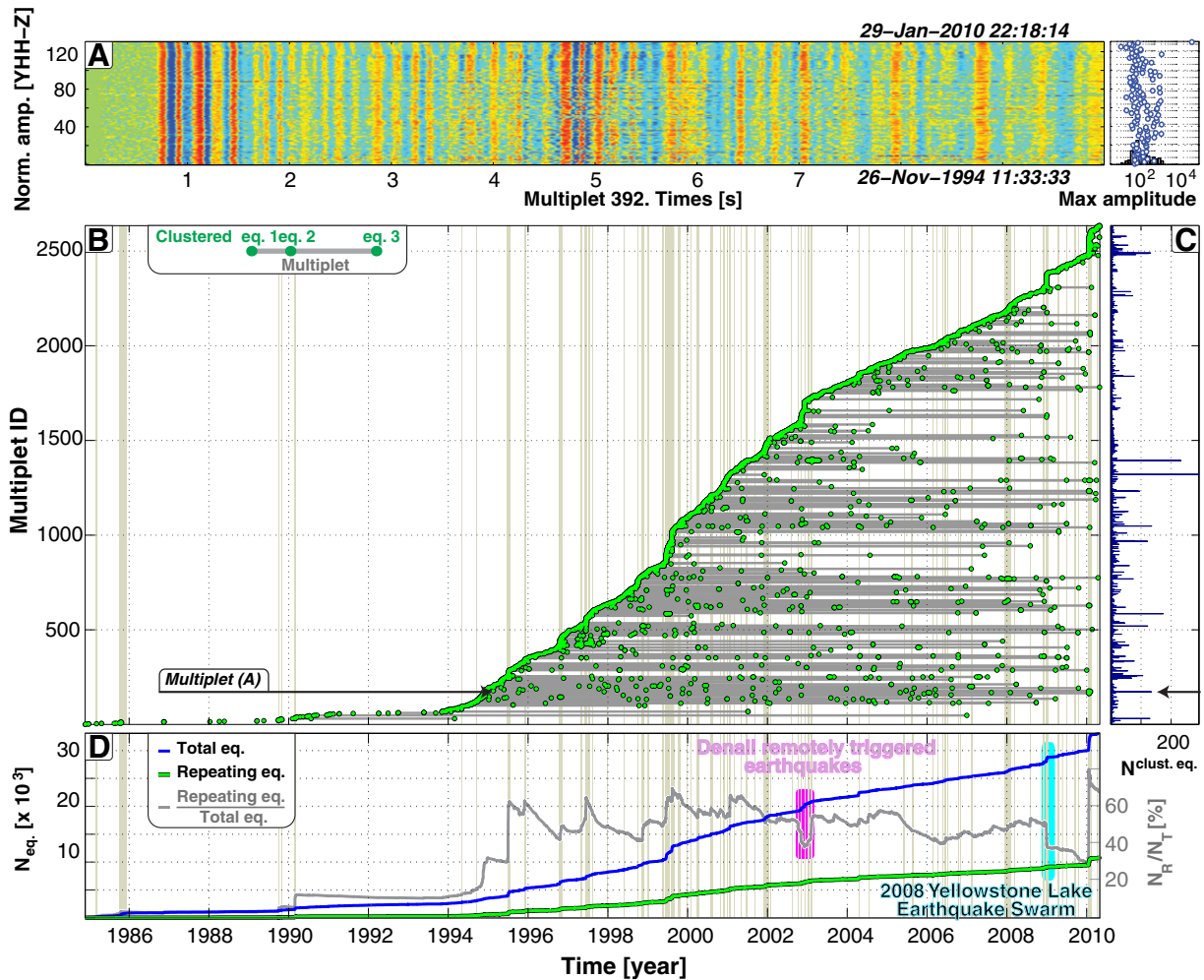
Fig. 2. Yellowstone multiplets chronology. A: waveforms of multiplet earthquakes (multiplet ID 382, from 1994 to 2010). Each seismic trace is plotted as a line normalized to ± 1, represented with the color-code blue for −1, red for 1. The absolute maximums of each trace are represented on the right side. B: dendrogram of the Yellowstone multiplets between 1984 and 2010. See legend for symbol code. The swarms identified by Farrell et al. (2009) are depicted as gray rectangles. Numbers of multiplet earthquakes are represented in C. D: temporal evolution of total earthquakes (bold blue), repeating earthquakes (green) and clustering rate (gray, right axis). Each swarm, except the 2008 Yellowstone Lake earthquake swarm, is a burst of repeating earthquakes.

Between 1994 and 2010, 15,466 of the 29,584 events (52%) were clustered. We identified 2654 multiplets, 1288 (48% of the 2654 multiplets) of which are composed of one doublet only and 1182 multiplets (44%) are composed of 3 to 10 earthquakes, and 236 multiplets (8%) of 11 to 50 earthquakes, 31 (1%) of more than 50 earthquakes. The largest multiplet is composed of 292 earthquakes. Fig. 2C shows that there is no correlation between the multiplet lifetime and its number of multiplet earthquakes.

Fig. 2D shows the temporal evolution of the repeating earthquake activity, or clustering rate that is defined as the ratio of the number of repeating earthquakes to the total number of earthquakes. The clustering rate decays between swarms, and abruptly increases during swarms. After 2001, Yellowstone swarm occurrence decreased from 6 to 3 swarms per year resulting in an overall decrease of the clustering rate. The YLES is the only swarm that was associated with a decrease in the clustering rate. Fig. 3 shows the spatial–temporal pattern of the clustering rate and its correlation to ground deformation.

3.2. Multiplets distribution and deformation

The clustering rate distribution from 1994 to 2010 is shown in Fig. 3A. The earthquakes in the northwestern part of the Yellowstone Plateau are composed of more than 50% repeating earthquakes. The

highest clustering rate in Yellowstone is associated with the Basin-Range normal faulting structures of the Hebgen Lake fault, Gallatin Range, and East Gallatin-Washburn fault zones (Figs. 1 and 3A). Within the Yellowstone caldera however the data reveal a lower relative clustering rate from 5% and 35%.

To examine the seismicity rates with crustal processes, we compare the temporal changes of the clustering rate (shown in Fig. 3B, C, and D) to variations in caldera ground motions determined by precise University of Utah GPS measurements (Puskas et al., 2007, Fig. 3E). From Chang et al. (2007) and Puskas et al. (2007) the ground velocities of the northwestern part of the caldera follow the opposite motion of the caldera (Mirror Plateau and the Sour Creek resurgent dome) from uplift to subsidence.

The 1996–1998 uplift episode (Fig. 3B) is associated with a clustering-rate decrease within the caldera and a clustering rate increase in the northwest. The 1998–2004 period of crustal subsidence (Fig. 3C) is associated with a slight increase of the clustering rate in the caldera and a clustering rate decrease in its northwestern vicinity. Moreover the 2004–2010 accelerated caldera uplift episode (Fig. 3D) is associated with a slight decrease in clustering rate within the caldera and a clustering rate increase in the northern caldera. The changes in clustering rate distributions of both uplift episodes are similar and opposite to the changes during caldera subsidence.
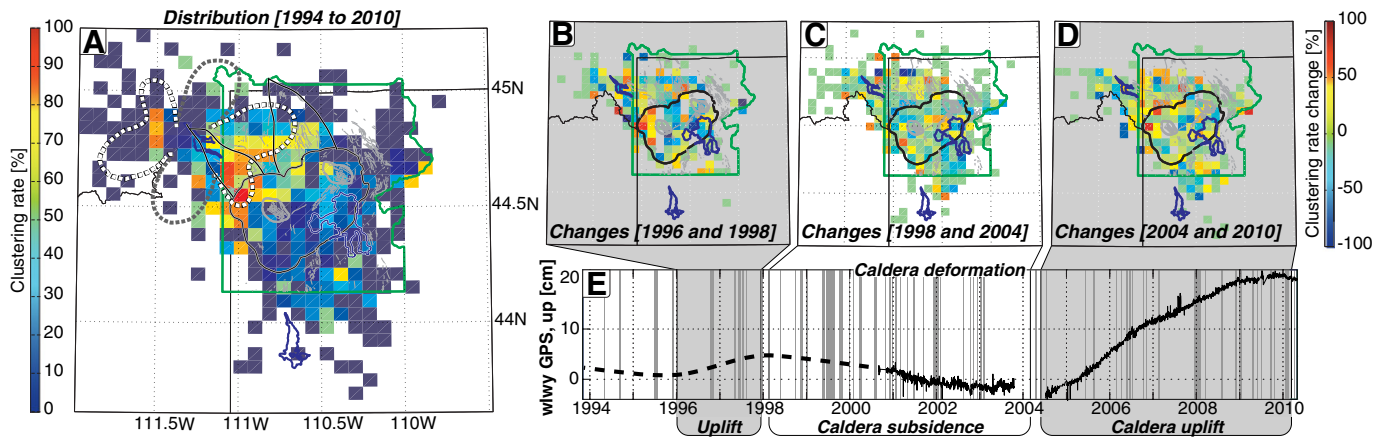
Fig. 3. Earthquake clustering rate distribution and temporal variations. A: map of clustering rate during the entire 1992–2010 time period. The northern vicinity of the caldera contains the most active multiplet generators. The white dash line represents the area of Coulomb static stress increase of 4 bars or more by the Mw7.3 Hebgen Lake earthquake of 1959 (gray dash line: area of a decrease of 4 bars or more). A is the reference pattern for change study in B, C and D. B: change from A during the 1996–1998 uplift episode. C: change from A during the 1998–2004 subsidence episode. D: change from A during the 2004–2010 uplift episode. E: caldera vertical ground deformation from GPS data with its maximum rate of uplift on the northside of the Sour Creek Dome, GPS station WLWY (see Chang et al., 2007; Puskas et al., 2007, for details). The swarms identified by Farrell et al. (2009) are depicted in E as gray rectangles.

Our results show that multiplets preferentially occur during crustal subsidence episodes.

3.3. Earthquake aftershock sequences

Foreshocks and aftershocks are usually studied at the temporal scale of an entire earthquake sequence. In this section, we highlight the foreshock and aftershock sequences of some multiplets, that will show variations from hours to years. Fig. 4-1a through 4a shows examples of seismic cycles of four kinds of multiplets. Fig. 4-1a represents the average evolution of the cumulative seismic moment in background multiplets. The background multiplets are defined as those without any multiplet earthquakes during swarms. Before being averaged, the evolution of the cumulative seismic moment of each multiplet is normalized in time and energy (the origin time and energy of the first multiplet earthquake is set at 0, the last is set at 1). The density of the cumulative seismic moment is depicted by gray dots in Fig. 4-1. The rate of released seismic moment per unit of time is indicated in gray (right axis of Fig. 4-1a). The background multiplets generally show a deceleration of the moment release, illustrating that background multiplets often release stress with main-shocks followed by aftershock sequences. But at the end of background multiplet sequences, a new phase of accelerated moment release begins.

The last phase shows that a minor part of background multiplets follows foreshock sequences before ending with a main-shock. Swarm multiplets (Fig. 4-2a) follow the same tendency as the background multiplets, but the foreshock sequences are less frequent than in background seismicity. The YLES sequence (Fig. 4-3a) is mostly composed of doublets, its multiplets are not consistent with any tectonic stress relaxation sequence but with a nearly constant relaxation rate. The multiplets seismic moment evolution in the MPES (Fig. 4-4a) is the same as other swarms.

Fig. 4-1b through 4b shows the stacked number of earthquakes per time (logarithmic) bin after (black line) and before (gray line) the main-shock. The main-shock of each multiplet is identified as the multiplet event of largest magnitude. The dominant doublet separation in background multiplets is one week; the secondary typical doublet separations are one hundred days and three to five years (Fig. 4-1b). Doublets during swarms (Fig. 4-2b) are generally separated by one day to a week. But, the YLES sequence is associated

with typical doublet separations from 16 h to one day (Fig. 4-3b). In Fig. 4-4b, the MPES shows the same major separation time as any other swarm.

We then compare the migration dynamics for the three identified sequences (AYES, the YLES and the MPES). This is done by modeling the possible sources of migrating stress field perturbations for the three swarms. Among the range of viable processes of migrating stress field perturbation, we investigate the intrusion of a mobile component in the crust of hydrothermal and magmatic fluids (Rubin, 1995) that can trigger a migrating seismogenic front instead of an expanding seismogenic blade-like shaped zone. The migration of the front seems the most consistent with short and migrating multiplets occurring without a main-shock as in the YLES however, other processes may also be viable.

4. Thermo-dynamical modeling of migrating earthquake swarms

In this section we summarize how Taisne and Tait (2011) employed analog laboratory experiments of fluid intrusions to obtain the mathematical description of the fluid dynamics of a modeled fluid intrusion that we scale to that of Yellowstone crustal conditions and migrating earthquake swarms. This work is based on the idea that bursts of earthquakes during seismic swarms would be a plausible seismic release because the solidification of the dike edge can retard the propagation, inducing strain and deformation by swelling over a constant area until the pressure increase within the fluid volume of the dike overcomes the strength of the solidified magma starting a new increment of propagation. Taisne and Tait (2011) experimented the injection of a wide range of fluid viscosities in an elastic host medium (gelatin) reduced model. The intrusion rate was directly determined by observations of the fluid body, i.e. the intruded area, seen through the transparent host medium. Using their observation of a wide range of intrusion compositions, they demonstrate a relationship that constrains the dependence of a given intrusion dynamic to the flux and temperature of injection (the relationship is given in Eq. (1) and detailed in Section 4.2).

In a real-earth case, the intruded volume cannot be directly imaged of course. But the dike intrusion could be approximated to the migration of its associated earthquake swarm front as it responds to the dike's perturbations of the ambient stress field
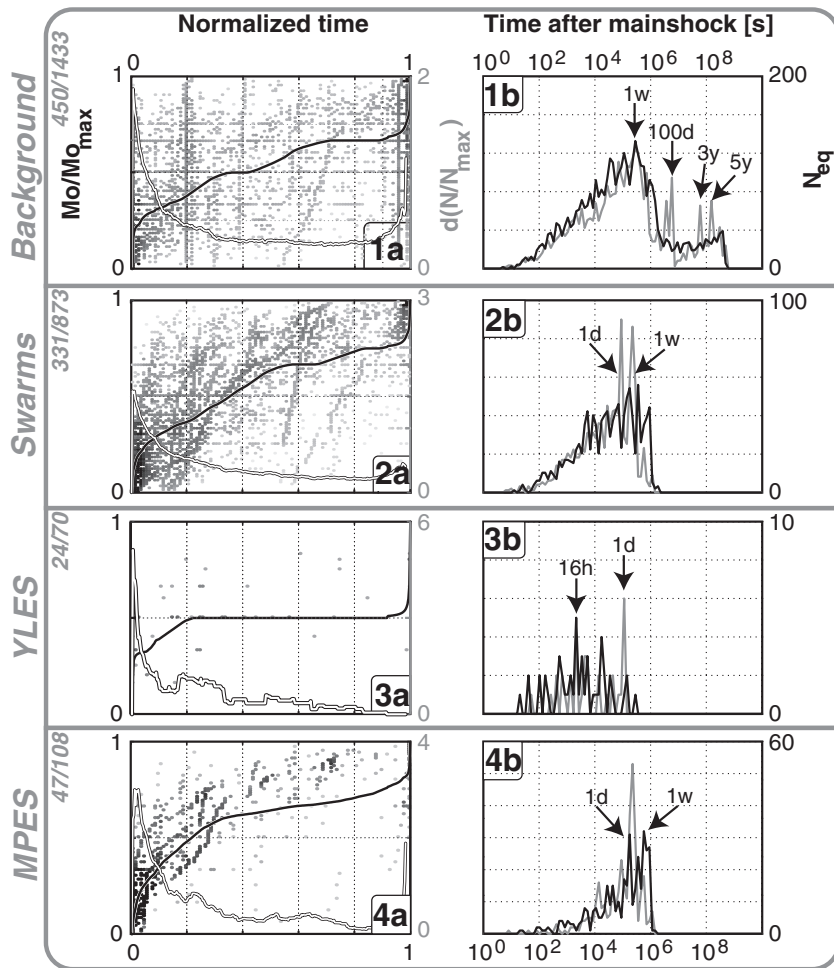
Fig. 4. Characterization of seismic cycles in multiplets. a: normalized evolution of cumulative seismic moment (black, right axis) and of moment rate (gray, right axis). b: rates of earthquakes following main-shocks (black) and before multiplet main-shocks (gray), rounded separation times are labeled for major peaks. 1: background multiplets, active only between swarms during the 1992–2010 time period (450 background multiplets, including more than three multiplet earthquakes, are represented). 2: swarm multiplets, active only during swarms during the 1992–2010 time period (331 swarm multiplets, including more than three multiplet earthquakes, are represented). 3: YLES multiplets, active only during the YLES (24 multiplets, including more than two multiplet earthquakes, are represented). 4: MPES multiplets, active only during the MPES (47 multiplets, including more than two multiplet earthquakes, are represented).

(Rubin et al., 1999). Also, Taisne and Tait (2011) consider the evolution of the cumulative number of earthquakes as a proxy for the evolution of the intruded volume. However, the analogy between intruded volume and earthquake swarms can probably be refined. In the next sections, we evaluated the Taisne and Tait (2011) modeling results using both total and repeating seismicity, which are shown in Figs. 5 through 7.

4.1. Swarm front migration data

Figs. 5 through 7 show the data (the cumulative earthquake numbers) used in our calculations and interpretations for the three Yellowstone migrating swarms (AYES, YLES and MPES). The evolution of the 1985 northwest caldera swarm (AYES) is represented in Fig. 5. The dendrogram (Fig. 5A) and the cumulative number of earthquakes (Fig. 5C) show that the AYES is composed of two phases labeled in Fig. 5A. Phase 1 (from October 6 to October 16) is composed of one set of long multiplets and a linear evolution of cumulative numbers of earthquakes (Fig. 5B). Phase 2 (from October 17 to October 22) exhibits only 5 daily and weekly multiplets during a northwestward migration of the earthquake sequence shaped like a horizontally oblong blade (after the swarm model by Waite and Smith, 2002). The migration coincides with bursts of orphan earthquakes and gives a stepwise evolution

in phase 2. During phase 2, Waite and Smith (2002) noted a maximum lateral migration rate of 150 m/day of the 1985 Yellowstone earthquake swarm toward the northwest. We use the cumulative total earthquake curve of phase 2 for modeling the swarm propagation properties.

The evolution of the 2008–2009 Yellowstone Lake swarm (YLES) is shown in Fig. 6. The dendrogram (Fig. 6A) as well as the cumulative number of earthquakes (Fig. 6B) show that the YLES follows a stepwise migration. The swarm evolution exhibited bursts of daily multiplets (in gray rectangles) and periods of reduced activity illustrated by steps in the cumulated number of earthquakes. Note that the 16 h of doublet separation (Fig. 4-3b) corresponds to the burst of repeating earthquakes. Few multiplets re-activated the same source volume before and after a period of seismic quiescence, resulting in the single-day doublet secondary separation in Fig. 4-3b. In contrast, the 2008 migration rate (1 km/day toward the north) is much faster than the 1985 migration rate (Farrell et al., 2010a, 2010b). We use the cumulated curves shown in Fig. 6B for modeling.

The evolution of the 2010 Madison Plateau swarm (MPES) is shown in Fig. 7. Sixteen earthquakes were recorded in the MPES area 2 days before the start on January 17, 2010 of the swarm that ended on February 5, 2010. The dendrogram (Fig. 7A) and the cumulative number of earthquakes (Fig. 7B) show that the
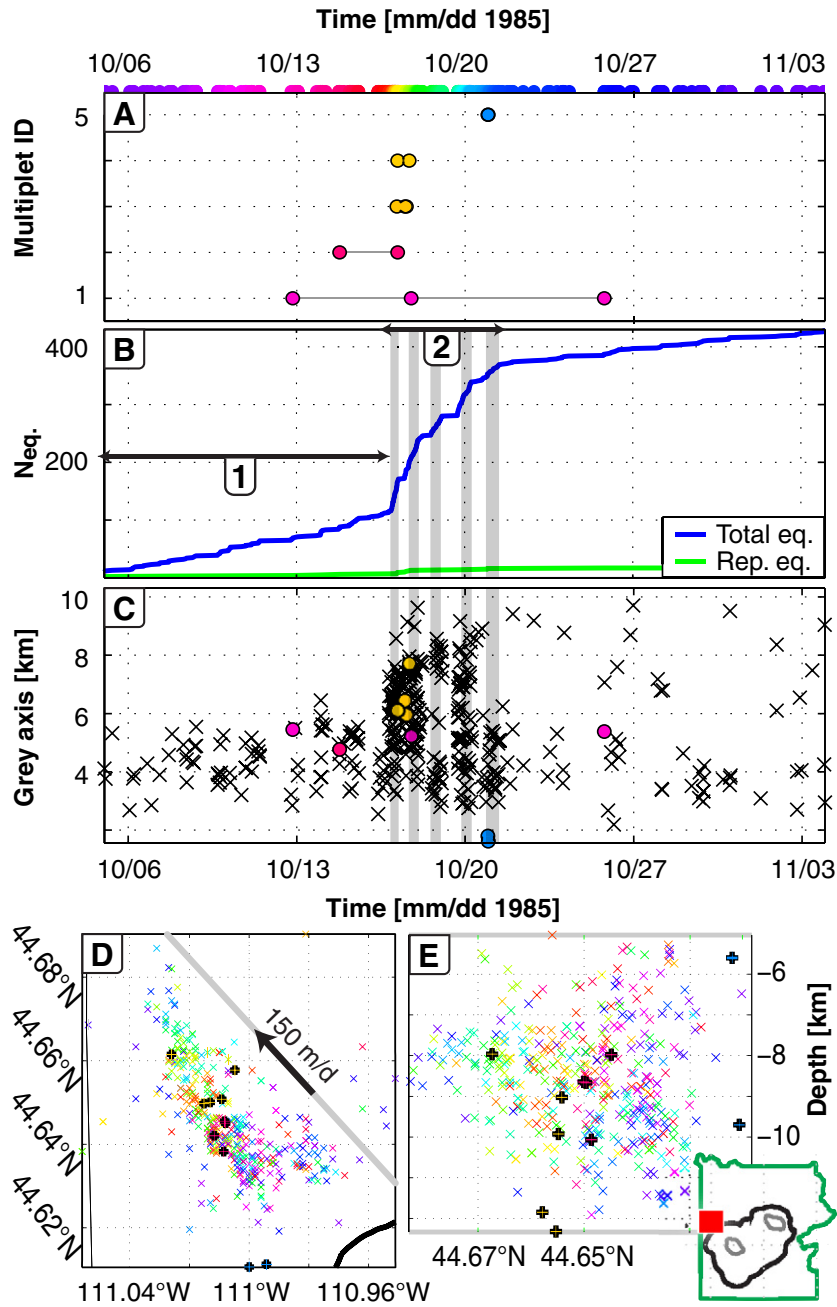
Fig. 5. The autumn 1985 Yellowstone earthquake swarm. A: dendrogram, the gray rectangles highlight migration steps. B: temporal evolution of total (blue) and repeating earthquakes (green). 1: first phase of non-migrating earthquake activity. 2: second phase of northwestern migrating earthquake activity (150 m per days). C: lateral migration of earthquakes in function of time. D, E: earthquake map and cross-section. Earthquakes are relocated with the double-difference hypocenter location code, hypoDD (Waldhauser and Ellsworth, 2000) in a 3D velocity model. Repeating earthquake colors are keyed to associated dendrogram (A, black bold crosses) and thin oblique crosses represent orphan earthquakes (color keyed in A).

MPES was a highly clustered swarm (60% clustering rate) composed of three main phases starting on January 17. As described in a Shelly et al. (2012) study of micro-earthquakes, the swarm first follows an outward migration during the first phase that ends in ~6 days (400 m/day northward, 300 m/day southward). The first phase evolution exhibits bursts of daily and weekly multiplets from January 19 to 20, 2010 (also shown in Fig. 4-4b). After a day of reduced activity, the center of earthquake activity moved to the deepest part of the swarm, 9 to 10 km deep, during the second phase. Activity diminished progressively before the third phase of earthquake nucleation on a second nearby area to the east of the swarm around 7 km deep (Fig. 7D and E). We use the cumulated curves of phase 1 for modeling.

4.2. Swarm front migration modeling

For better understanding of the modeling approach we summarize the fluid analog modeling method of Taisne and Tait (2011) in three steps: parameter normalization, fitting, and sizing. Earthquake cumulative curves are normalized in time and in earthquake total number to obtain Figs. 8A through 10A which can be compared to each other. Each dimensionless curve is used to produce a histogram of earthquake rates, τ, (Figs. 8B–10B), the lower rates reflecting the flatter parts of the initial curves. The normalized integrals of the cumulative histogram rates, η, show the stepwise incremental migration in each of the three swarms (Figs. 8C through 10C). The steeper the onset of the curves is in Figs. 8C–10C, the more the earthquake migration is stepwise. The
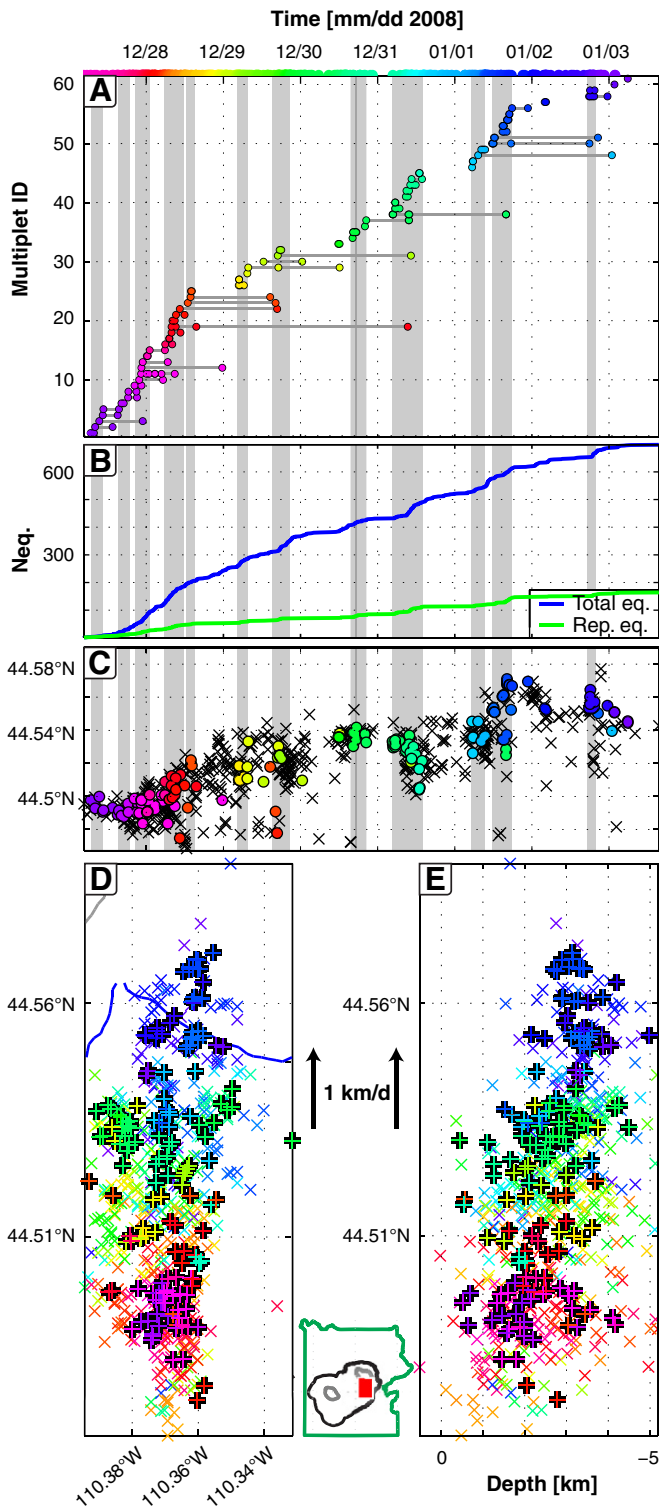
Fig. 6. The 2008 Yellowstone Lake earthquake swarm. Same letter code as Fig. 5.
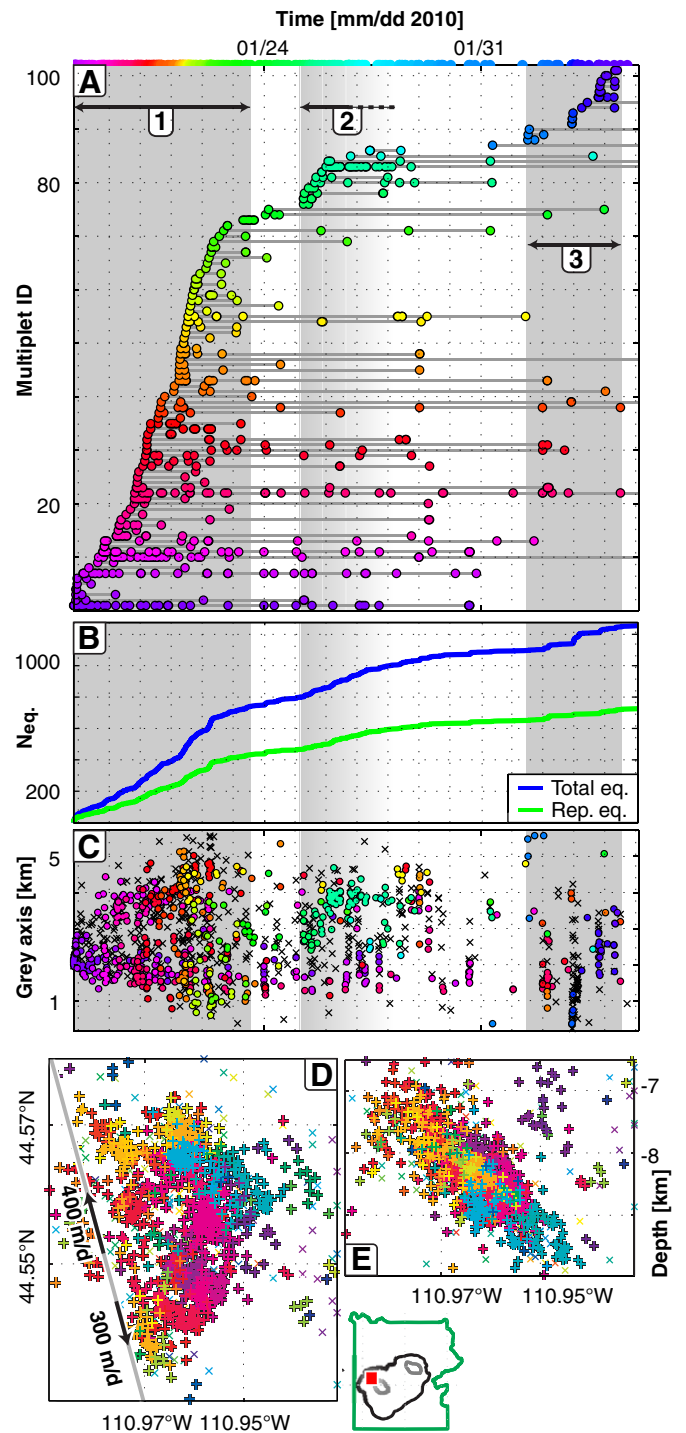

Fig. 7. The 2010 Madison Plateau earthquake swarm. Same letter code as Fig. 5. 1: first phase of outward migrating earthquake activity. 2: second phase of activity shift to the base of the swarm. 3: third phase of activity shift to a parallel system.

dimensionless representations in Figs. 8C through 10C can be fitted by Eq. (1) from Taisne and Tait (2011), with four dependent parameters.

$$\eta/\eta_{\text{Total}} = \alpha(1 - \exp(-\lambda\tau/\tau_{\text{max}})) + (1-\alpha)1/2(1 + \text{erf}((\tau/\tau_{\text{max}} - \mu_G)/\sigma\sqrt{2}) \quad (1)$$

where:

α represents the proportion of values between the propagation being stopped ($\alpha = 0$) and continuous propagation ($\alpha = 1$),

λ is a free fitting parameter (positive integer),

μ_G is the average normalized seismicity rate ([0, 1]) and

σ is the standard deviation of normalized seismicity rates (positive integer).

These four parameters are given in the legend of Figs. 8C, 9B and 10C. Among these four parameters α and μ_G are sensitive to the dimensionless temperature, and to the dimensionless flux. The density and solidus of the intruded material are the most important parameters for the calculation of the physical values of flux and temperature.
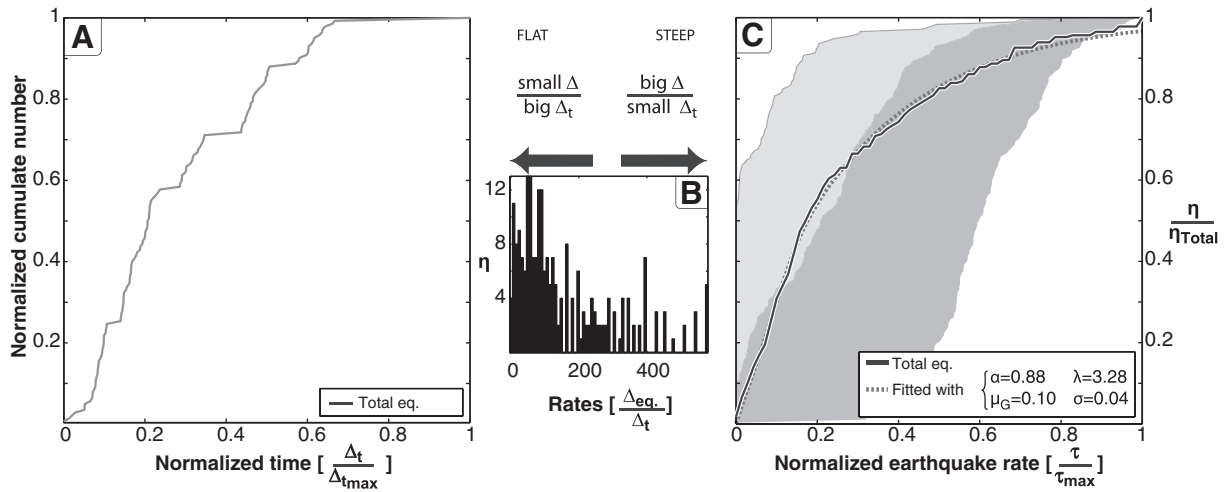
Fig. 8. Modeling of the Autumn 1985 Yellowstone Swarm. A: cumulative number of earthquakes, normalized by their final values. Dimensionless curves (A) are used for histograms of earthquake rates (B). C: normalized integral of B. This curve is fitted with a theoretical description of solidifying intrusions (Eq. (1) from Taisne and Tait, 2011). A thin gray line represents the fitting curve. The domain of solidifying intrusions is the light gray area and the domain of continuous intrusion is the dark gray area. Adjustment parameters α and μ$_G$ are used in flux and temperature calculations. α represents the proportion of values between the propagation being stopped (α = 0) and continuous propagation (α = 1), μ$_G$ is the average normalized seismicity rate ([0, 1]).

The source of the migrating stress field perturbation is hypothesized as a hydrothermal fluid intrusion, a rhyolite or a basalt intrusion (with density intervals, respectively, [1, 1.1], [2.1, 2.4], and [2.6, 2.7] in kg·m^{-3}, Bottinga and Weill, 1970, and in Shane et al., 2007). We used intervals of density and our results are intervals of physical fluxes and temperatures for the three cases of intruded material (in °C and cubic meters per second in Table 1). Then we use the average height of the seismic swarm (H) as an approximation of the average height of the final intrusion, the migration rate (R) as an approximation of the intrusion velocity and the physical flux values (Q) to define the dike width (w) of each intrusion following Eq. (2).

$$w = Q/(H R) \qquad (2)$$

5. Thermodynamic properties of swarm migration

5.1. The autumn 1985 Yellowstone earthquake swarm

Fig. 8C shows the dimensionless representations of the total earthquakes which are mostly inside the area of continuous fluid migration (dark gray area on Fig. 8C). The continuous oblong blade-like shaped pattern of the 1985 earthquake migration could be induced by non-solidifying intruding material, or by a high flux of solidifying material. As an illustration, in Table 1A, numerical applications of our dimensionless flux and temperature measurements lead to high fluxes of magma and flux of hydrothermal fluids in the order of a cubic meter per second. Considering the flux and width results, the hydrothermal fluid solution presents both advantages of low injection flux values and sub-metric dike width. We prefer this solution because of consistency with the slow fluid migration rate and other observations detailed in the Discussion section.

5.2. The 2008–2009 Yellowstone Lake earthquake swarm

In Fig. 9A, B, and C the cumulative curve of repeating earthquakes (gray) during the YLES shows a high proportion of aseismic episodes meaning that each intrusion step takes a relatively longer time compared to total earthquakes. This tendency involved lower injection fluxes in Table 1B for the repeating earthquake results than for the total earthquake results, but slightly higher temperatures. Our estimate

for a hydrothermal fluid intrusion would have an injection flux of 0.5 to 0.9 m^3/s. Due to its low density, a hydrothermal fluid intrusion could occur with low injection flux and low dike width from 1 to 2 cm. In contrast, a basaltic magma dike model would have a temperature between 900 °C and 1000 °C. Basalt being denser than the rhyolitic host rock, the basaltic dike would intrude at a high flux value over ~10 m^3/s.

To fit the models with the dimensions and duration of the observed migrating swarm, the modeled dike would have to be at least 20 cm thick. An intrusion of rhyolitic magma would require a temperature of 750 °C to 900 °C. Such an intrusion requires an average injection flux of 1 to 5 m^3/s. The average width of this hypothesized dike is 3 to 13 cm. Considering the flux and width results, the rhyolitic magma solution presents both advantages of reasonable flux values and reasonable dike width. In the Discussion, we prefer this latter solution especially because of its consistency with the rapid migration rate and slight ground deformation.

5.3. The 2010 Madison Plateau earthquake swarm

As shown in Fig. 10A and in the fitting values of Fig. 10C, the average normalized earthquake rate (μG) during the MPES is higher for repeating earthquakes than for that of the total earthquakes. With earthquake rate being directly proportional to flux, we employed the results from the total number of earthquakes that minimizes the flux values. Repeating earthquake data would induce high injection flux estimates, several times over 10 m^3/s for magmatic intrusions. This is opposite to the result for the YLES, where total earthquakes data notably decreases our results to be more consistent with experimental values of earthquake rates found in Taisne and Tait (2011). The MPES and YLES have to nucleate in a different way, from different types of stress perturbation sources.

Our estimate for hydrothermal fluid intrusions during the MPES suggests a low injection flux that is less than 1 cubic meter per second. Due to its low density, a hydrothermal fluid intrusion could only require a dike a centimeter in thickness. A basaltic dike model would have a temperature between 1000 °C and 1100 °C and intrude at a flux value over 5 m^3/s in a dike, at least, 3 cm thick. An intrusion of rhyolitic magma should have a temperature of 800 °C to 900 °C and an average injection flux of 0.6 to 2.7 m^3/s in a dike 4 to 17 cm thick. In the Discussion, we will not choose a preferred solution because the deformation data show no signal that could help in
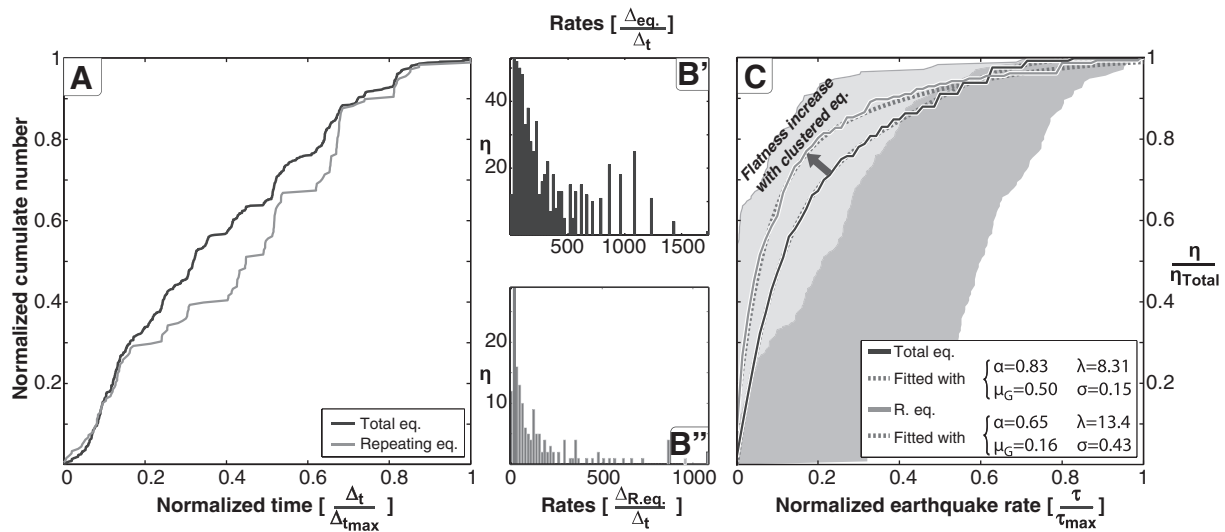
Fig. 9. Modeling of the 2008 Yellowstone Lake earthquake swarm. Same letter code as Fig. 6. Black, B′: total earthquake data. Gray, B″: repeating earthquake data.

estimating a realistic intrusion width without confirming an absence of any crustal deformation at the time of the 2010 Madison Plateau swarm (Puskas, personal communication and Puskas et al., 2012).

6. Discussion

Earthquakes and earthquake swarms throughout Yellowstone occur under the influence of a regional uniform N-S to NE-SW extensional stress field (Waite and Smith, 2004; Puskas et al., 2007). This background stress is perturbed by Yellowstone's inflation–deflation features (hypothesized as inflating–deflating dike or magmatic to hydrothermal fluid reservoir) whose variable stress loading affects the earthquake clustering rate of Yellowstone. During the last 30 + years of modern seismic recording, the Yellowstone system has only revealed two earthquake sequences, one during the Autumn 1985 Yellowstone earthquake swarm and one during the 2008–2009 Yellowstone Lake earthquake swarm, that could be directly attributed to magmatic and hydrothermal processes.

6.1. Yellowstone earthquake clustering rates

Seismicity of the Yellowstone caldera area reveals an average clustering rate of 37% (i.e. the proportion of repeating earthquake in total seismicity) while outside the caldera is showing a 75% average. From a global perspective the Yellowstone caldera clustering rate is in agreement with rates in other active volcanic systems. For example, clustering rates of 24% have been found in Fogo volcano (Cape Verde, from 2003 to 2004 Martini et al., 2009), 35% in Etna, Italy, (1991- 1993 Brancato and Gresta, 2003), 37% in Montserrat, British West Indies (1995–1996 Rowe et al., 2004), 25 to 30% at Kilauea, Hawaii (US, 1988–1999 Got and Okubo, 2003) and 26% in the caldera of Deception Island volcano, West Antarctica, (1999, Carmona et al., 2010).

The high clustering rate of 75% in the Hebgen Lake-western Yellowstone area is also in agreement with similar studies of active tectonic regions. The subduction zone of Nicoya Peninsula, Costa Rica, has a rate of 81% from 2000 to 2001 (Hansen et al., 2006). The San Andreas fault, California, has been shown to have a rate of 21% from 1984 to 2003 (Waldhauser and Schaff, 2008). As observed in the large-scale study
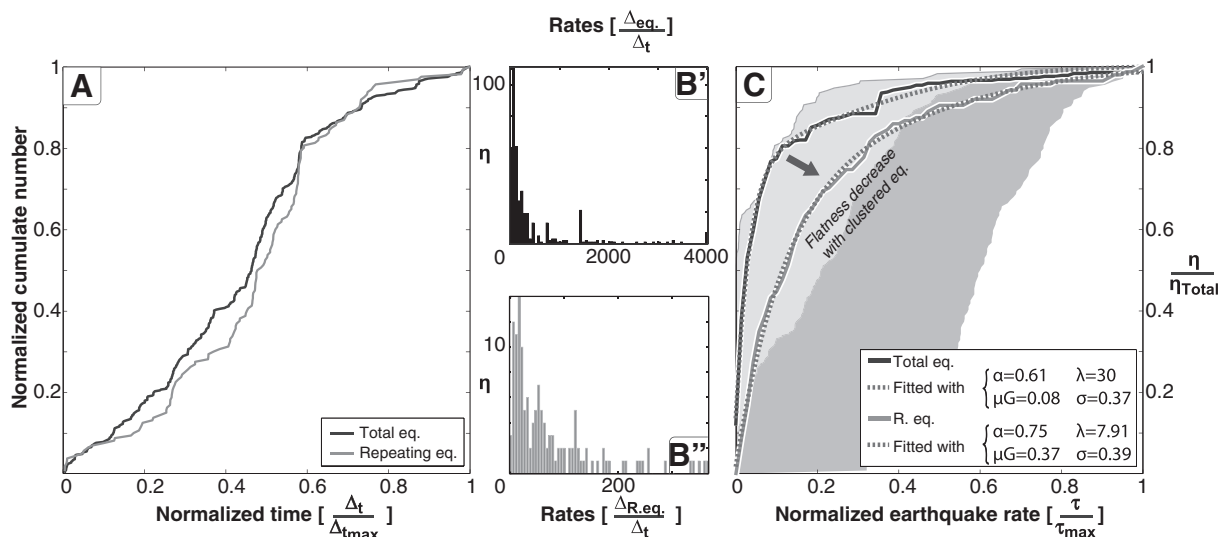

Fig. 10. Modeling of the 2010 Madison Plateau Earthquake Swarm. Same letter code as Fig. 7.

Table 1

Numerical calculation of average temperatures, injection fluxes, and dike widths associated with the 1985 northwest caldera and the 2008 Yellowstone Lake earthquake swarms, for three types of plausible intruding material: rhyolitic magma, basaltic magma, and hydrothermal fluid (H.F.) A: Autumn 1985 Yellowstone earthquake swarm. B: 2008 Yellowstone Lake earthquake swarm.

		Rhyolite	Basalt	H.F.	
A					
Temperature, T_m	min.	758	962	403	[°C]
	max.	880	1012	505	
Flux, Q	min.	1.4	11.4	0.5	[m³·s⁻¹]
	max.	5.9	1591.6	1.0	
Width, w	min.	0.4	3.3	0.1	[m]
	max.	1.7	458.4	0.3	
B					
Temperature, T_m	min.	783	995	412	[°C]
	max.	910	1048	518	
Flux, Q	min.	1.2	10	0.4	[m³·s⁻¹]
	max.	5.2	1404	0.9	
Width, w	min.	0.03	0.20	0.01	[m]
	max.	0.13	34.70	0.02	
C					
Temperature, T_m	min.	825	1052	427	[°C]
	max.	961	1109	541	
Flux, Q	min.	0.6	5.2	0.2	[m³·s⁻¹]
	max.	2.7	724	0.5	
Width, w	min.	0.04	0.3	0.01	[m]
	max.	0.17	44.7	0.03	

of Waldhauser and Schaff (2008) for the San Andreas fault, our results show that the long-term seismic monitoring and data archiving lead to continued improvement in the multiplet database, implying continued improvement of their source parameters.

6.2. Stress states

Mogi (1963) and Sykes (1970) defined earthquake swarms to consist of a series of earthquakes closely clustered in space and time and lacking a clear main-shock. Mogi (1963) established three models of seismic rupture (aftershock sequences, both foreshock and aftershock sequences and sequences lacking a main-shock) and related them to three kinds of geological context (homogeneous, heterogeneous, extremely heterogeneous) and stress states (uniform, non-uniform, concentrated). The transition between the three categories is continuous. Our investigation of Yellowstone multiplets shows that they correspond dominantly to aftershock sequences. A minor seismic energy release through foreshocks has been observed in our study; preferentially in background multiplets to the detriment of swarm multiplets mostly made of aftershock sequences. Following Mogi (1963), Yellowstone multiplets are likely triggered in a heterogeneous medium superimposed on the more uniform regional stress field dominated by extensional normal faulting earthquakes. The 2008–2009 Yellowstone Lake swarm is the only swarm evaluated without a discernible main-shock. Considering Mogi's model, only the YLES responds to a concentrated stress perturbation in a very heterogeneous medium.

Chang and Smith (2002), compared the crustal deformation pattern from GPS measurements and earthquake occurrence of the Yellowstone caldera and showed that a major part of the 1959–1995 earthquakes were located in the areas of increased Coulomb failure stress induced by the 1959 Hebgen Lake, Montana, Mw7.3 earthquake located on the west side of the Yellowstone Plateau and ~20 km from the Yellowstone caldera. These results demonstrated a strong spatial correlation between the Mw7.3 failure-stress change and Yellowstone's earthquake distribution. The high clustering rate anomaly in the Hebgen Lake region (Fig. 3) includes the southern

part of the area of increased failure stress induced by the 1959 Hebgen Lake earthquake. Our results suggest a spatial correlation between the 1959 induced static-stress change and Yellowstone's multiplet distribution. Our results thus suggest that the Hegben Lake area multiplets could be continued aftershocks to the 1959 Hebgen Lake main-shock.

6.3. Insights on structural evolution during swarms and crustal uplift

The relatively slow decay of clustering rates between swarms and the following rapid increase of clustering rate during swarms provides insightful information about tectonic stress accumulation (see Fig. 2B and D). A clustering rate decay mechanism corresponds to a relative increase of "orphan" earthquake activity. Orphan earthquakes occur only one time during our two decades study and are single seismic sources and potential future multiplets. They may indicate the rupture of intact rocks or of partially healed pre-existing faults. If a decrease of clustering rate is interpreted as an episode of neo-tectonic activity and if an increase of clustering rate is interpreted as an episode of fault reactivation, our results suggest that a neo-tectonic episode accompanies the pre-swarm stress accumulation. In this hypothesis, the clustering rate increase during swarms is consistent with the idea of swarms triggered by the rupture of a pre-existing preferential axis of stress release.

Our results also suggest that multiplets occur preferentially in areas dominated by crustal subsidence. We show the first well-documented observations of the co-evolution between ground motion and multiplets, in good agreement with the results of crustal deformation determinations by GPS of Puskas et al. (2012) that highlight similarities in the stress driving mechanisms between earthquake distribution and models of chamber stress perturbations. Chang et al. (2007) and Puskas et al. (2007) also investigated earthquake activity along a detail analysis of ground deformation in Yellowstone without revealing any correlation with deformation. As shown by Puskas et al. (2007), the orientation of maximum extensional strain rate in Yellowstone is consistent with Basin and Range extension and that ground deformation in Yellowstone is the product of regional extension superimposed by stress perturbations caused by the Yellowstone magma dynamic. In addition to the work of Puskas et al (2007), our study shows that the magmatic system and earthquake activity are coupled. We interpret an increase of clustering rate as a stress activation of pre-existing faults to the detriment of developing young or new seismic faults. Our preferred model is that an increase of earthquake clustering rates during subsidence suggests the preferential activation of Basin and Range pre-existing extensional structures (mainly composed of north–south normal faults). During uplift (from 1996 to1998 and from 2004 to 2010), this extensional stress regime affects earthquakes in the Hebgen and Gallatin areas that trigger mostly repeating earthquakes, and other young structures could be activated to trigger mostly orphan earthquakes (post-caldera fault networks in Fig. 3: Elephant Back fault system, Mallard Lake and Sour Creek resurgent domes). The Long Valley caldera, California, is a good analog of Yellowstone, and shows a strong correlation of earthquakes and deformation. In the systematic review of earthquakes and deformation by Hill et al. (2003), episodes of seismic quiescence in Long Valley caldera have been identified prior to the onset of periods of uplift. Similarly, a detailed analysis of crustal deformation and earthquakes by Feng and Newman (2009) showed that the peak seismicity rates in Long Valley caldera coincide with periods of maximum inflation rates. Hill et al. (2003) also observed that uplift episodes are associated with increases in earthquake swarm activity, b-value increases, and the lack of main-shock–aftershock sequences. In the absence of b-value coherent change (Farrell, 2007) and of large aftershock sequences in Yellowstone, investigating the clustering rate in Long Valley and in other volcanoes would be interesting.

6.4. Hydrothermal fluid interaction of the autumn 1985 earthquake swarm

The autumn 1985 northwest Yellowstone caldera earthquake swarm, the 2008–2009 Yellowstone Lake earthquake swarm and the 2010 Madison Plateau earthquake swarm were the most notable swarms with migrating earthquake fronts in Yellowstone (Smith et al., 2009). The three episodes, however, differ in several aspects. The AYES had a migration rate of 150 m/day over four days (Waite and Smith, 2002), and 350 m/day over 6 days for the MPES, while the YLES had a 1 km/day migration rate over 10 days (Farrell et al., 2010a, 2010b). As explained in Section 4, the AYES started with a 10 day-long phase of non-migrating rupture (from October 6 to October 16, Fig. 5). This first phase could be interpreted as a tectonic related swarm (i.e., a swarm that nucleated along an optimally-oriented fault, like the other non-migrating swarms). However the five-day, fast-migrating phase (from October 17 to October 22, Fig. 5) shows a stepwise evolution of the cumulative number of earthquakes and a low clustering rate. This migration appears to be relatively close to a continuous migration as defined in the analogue models of fluid dynamics by Taisne and Tait (2011).

It provides an interesting result, namely that the more acceptable injection flux estimate (lower than 1 m^3/s) is given by hypothesizing the slow injection of a hydrothermal fluid mostly composed of liquid water as a migrating stress perturbation source. This slow hydrothermal fluid intrusion hypothesis is in agreement with the slow migration rate of Waite and Smith (2002). Waite and Smith (2002) proposed that the AYES was induced by hydrothermal fluid motions, increasing pore fluid pressure and reducing the effective normal stress as explained in Fournier (1999). They also considered the idea of a magmatic dike and of a water-filled dike as inconsistent with the observations and model results. Waite and Smith (2002) explain that, following the results of Rubin's (1995) models of Hawaii swarm properties the viscosity calculated for magmatic dike emplacement would imply a meter thick dike and viscosity of a rhyolitic magma but such dikes are not likely to intrude in cold and shallow medium. Also, the width of a water-fluid dike that satisfies the migration rate would be too narrow to induce the observed seismicity and focal mechanisms.

We adopt a conceptual model based on the same idea as Waite and Smith (2002) and Fournier (1999) in Fig. 11-1 to explain the 1985 northwest caldera swarm. It is important to note that this swarm occurred adjacent to the mapped caldera boundary, where the hydrothermal system is expected to deepen from south to north, i.e. outward of the caldera (as schematized in Fig. 11-1 by the schematic blue area). The AYES initiates as a tectonic swarm (Fig. 11-1a), but it reaches and destabilizes the hydrothermal system after about 10 days. Because of the fracture-flow modification from the swarm and because intrusion tends to be captured by damaged zones (Rubin, 1992) hypothesizing that the hydrothermal fluids flow outward from the caldera, toward lower fluid pressure and the damaged zone. This process induces an increase of pore pressure that facilitates rupture in the injection direction. Each rupture step and related fracture modification captures hydrothermal fluids because of a lower pressure gradient. This self-maintained migration (Fig. 11-2) lasted until the thin blade of hydrothermal fluid extended enough to disconnect from the hydrothermal system.

6.5. Multiplet triggering of the 2008–2009 Yellowstone Lake magma intrusion

After reviewing the 25-year history of Yellowstone swarms (Farrell, 2007) the 2008–2009 Yellowstone Lake earthquake swarm is the only magmatic (magma-hydrothermal fluid) related swarm that has been identified by contemporary Yellowstone geophysical studies. A key characteristic of the YLES is the lack of main-shock in its multiplets suggesting that earthquakes are induced by an extremely concentrated stress perturbation (Mogi, 1963). A second characteristic of the YLES is

the migrating multiplets with daily durations occurring in bursts that succeed each other with very few links (Fig. 6A). It is evident that the migrating stress perturbation is associated with fracture locking or destruction of the oldest multiplets. This observation is in good agreement with the observations made from the detailed seismic analysis of the swarm by Farrell et al. (2010a, 2010b). Considering these two major characteristics specific to the YLES, we cannot interpret this atypical swarm as the AYES nor as the other tectonic swarms. Finally, the YLES revealed a stepwise migration pattern, typical of intrusion of solidifying material, allowing us to measure an injection flux that is compatible with rhyolitic magma (see also Farrell et al., 2010a, 2010b).

Farrell et al. (2010a, 2010b) used the time duration of the swarm to estimate the magma dike width and length that corresponds to such a total solidification time. However, the model of Farrell et al. (2010a, 2010b) did not take into account the effect of an advective flux of magma that would increase the solidification time of a given dike, or decrease the width of the dike for a given solidification time. Thus, the width estimations of Farrell et al. (2010a, 2010b) give maximum estimates of dike widths of 2 m for basalt and 1 m for rhyolite, respectively. Farrell et al. (2010a, 2010b) also employed the observed GPS observation of crustal motion of the Yellowstone Lake area that reflected dominant westward extension of 3 to 7 mm. This property was used to model the magma dike width. This elastic deformation model does not take into account the effect of a viscoelastic crust. Such behavior could accommodate a minor percentage of stress in plastic deformation and energy dissipation. Thus, the width estimations of Farrell et al. (2010a, 2010b) give minimal dike widths of 1.5 to 9.7 cm for the bottom and top of the dike, respectively that is in good agreement with the seismic moment tensor for a largest and early shock, Mw4.1, at the base of the swarm that shows an opening of 9.6 cm.

In Table 1B, solutions with a plausible range of widths (shown) for given geologic flow models can fit the acceptable width interval (1.5 cm to one or two meters) for the YLES. However the rhyolitic melt solution gives the best agreement with the width interval and an acceptable injection flux value. An injection flux lower than a cubic meter per second of hydrothermal fluids would not be sufficient to induce seismicity or a rock fracturing migration. An injection flux over 10 m^3/s of basaltic magma would be capable of triggering the observed earthquakes but it would also intrude in a wider dike than acceptable, definitively wider than the inversion results of Farrell et al. (2010a, 2010b). The rhyolitic magma solution thus represents both reasonable flux values (1.2 to 5.2 m^3/s) and reasonable dike width (3 to 13 cm) for the migration properties of the 2008–2009 Yellowstone Lake swarm. Such dike thickness is in the observed range reported by Rubin (1995) but relatively small compared to rhyolite dike openings in Taupo, New Zealand (Seebeck and Nicol, 2009), Deception Island caldera, Antarctica (Baraldo and Rinaldi, 2000), or in Long Valley caldera, California (Reches and Fink, 1988). A thin dike could explain why the intrusion did not break the surface, because the magma buoyancy of a thin dike would not overcome the decrease in magma pressure during shallowing. Note that the high heat flow of the Yellowstone Lake area estimated to exceed ~20,000 mW m^{-2} (Morgan et al., 1977) would result in elevated crustal temperatures of the seismogenic layer that could promote rhyolite intrusion, which would be unlikely in cold medium.

Our seismo-magmatic model explaining the origin of the YLES is represented in Fig. 11-2. Earthquakes and multiplets are triggered by the stress perturbation at the head of a migrating rhyolitic magma intrusion; its first intrusion step is represented in Fig. 11-2A. In Fig. 11-2B, the intrusion edge freezes and stops. Swelling of the dike reactivates the same multiplets as in 2A and triggers orphan earthquakes. The magma injection flux breaks the solidified edge giving a burst of earthquakes (Fig. 11-2C). The edge rupture allows a second step of intrusion and the multiplets are destroyed (Fig. 11-2D). Both multiplets and orphan earthquakes occur during edge rupture but mostly orphan earthquakes occur during the swelling. Multiplets best reflect the intrusion step-wise propagation dynamic. Using Eq. (1) of
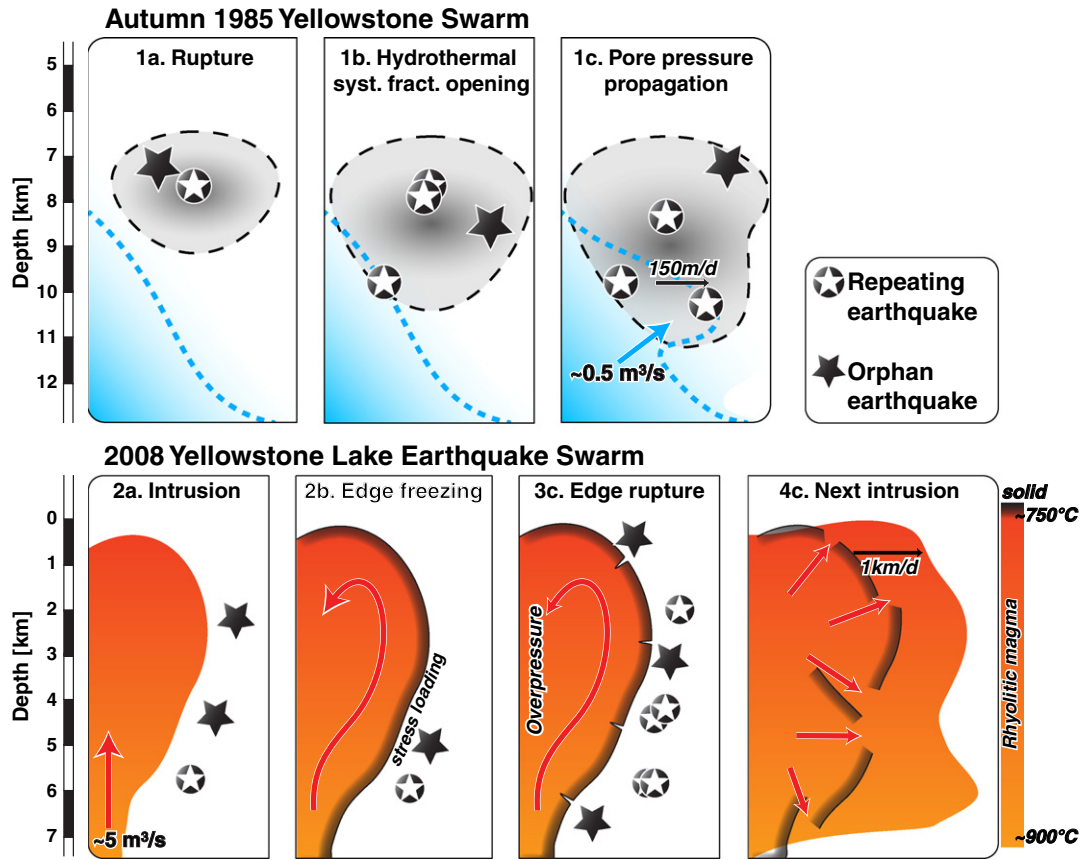
Fig. 11. Conceptual models of the 1985 and 2008 migrating swarms. Cross-section schemas along migration directions. Star: orphan earthquake. Circled star: repeating earthquakes. See discussion for details. 1: As suggested by Waite and Smith (2002), the AYES swarm starts with a tectonic stress relaxation phase (1a, rupture area in gray, hydrothermal system in blue). When the rupture reaches the hydrothermal system (1b), the AYES migrates 150 m/day, possibly around a blade of hydrothermal fluid (with an injection flux of ~0.5 m^3/s, diagram 1c). 2: As suggested by Farrell et al. (2010a, 2010b), a rhyolitic dike with edge freezing-failure cycles is our best hypothesis to model the dynamic of the 2008 earthquake migration (of 1 km/day on average). The migration stress perturbation is possibly due to a rhyolite dike intrusion (with a flux of 5 m^3/day, diagram 2a, orange area). The stress accumulation before each earthquake burst would correspond to freezing of the intrusion edge (2b, dark contour). We observed a dominance of orphan earthquakes during the two later steps. Each burst of earthquakes is dominated by repeating earthquakes corresponding to the failure of the dike edge that lead to the next migration step.

Rubin (1995), a shear modulus of 3×10^4 MPa, a Poisson's ratio of 0.35, and our calculated rhyolite dike width, we estimate the pressure in the dike between 0.2 and 1.8 MPa.

6.6. The 2010 Madison Plateau earthquake swarm rupture propagation

As explained in Section 4, the MPES starts with a 6-day-long phase of outward propagation of ruptures (from January 17 to 23, Fig. 7) on an east–northeast dipping plan. This plane is consistent with the southeast projection of the Hebgen Lake fault zone (Christiansen, 2001) toward the Madison Plateau area as a north-eastern conjugate fault. In our opinion, the MPES migration is best interpreted as a dominant tectonic related swarm consistent with observations of aftershock sequences (Fig. 4-4a) as already de-scribed in Japan (Imoto and Kishimoto, 1977) and South America (Holtkamp et al., 2011). The MPES initial phase also expands in bursts at an average rate of 350 m/day, which is important to com-pare. The 1985 AYES and the 2010 MPES have both relatively slow migration rates (respectively 150 m/day and 350 m/day) during several days (respectively 4 and 6 days) before ending progressively in the following weeks or months (respectively 3 months and 21 days). They also expand as a oblong blade-like shaped body, the whole swarm area being active during each migration increment, and does not move as a front.

The YLES migrates as a front of earthquakes (only the head of the swarm is active), that is one of the characteristics of a magma intrusion. The 2008 YLES and the 2010 MPES have opposite cluster-ing rates. For the MPES, the migration of orphan earthquakes is more stepwise than the repeating earthquakes. Repeating earth-quakes are less induced by the migration source in the MPES case than in the YLES case. The similarity of the migration style of the MPES with the AYES and the importance of the burst of orphan earthquakes that miss the YLES could suggest that the MPES is based, as the AYES, on a tectonic rupture, the propagation of which being promoted by fluid migration from tectonically fractured areas to surrounding pre-existing fault segments. This model is in partial agreement with Shelly et al. (2012) that consider the average migration rate of 350 m/day as primarily driven by hydrothermal fluid flow. As Waite and Smith (2002), we consider that the width of the water-fluid dike that satisfies the observed migration rate would be too narrow to induce by itself the observed seismicity.

The MPES probably occurred in the Yellowstone hydrothermal system without the lateral fluid pressure gradient of the AYES case. The outward propagating patches of weekly multiplets of Fig. 7 would correspond to fault segments that focus the rupture for a cer-tain time with aftershock sequences (Fig. 4-4a) before the transfer of activity in bursts of orphan earthquakes. We were able to model this burst as being triggered by migration of a cubic meter per second of hydrothermal fluids through centimeter thick cracks in Section 5.3. Activity transfer by orphan earthquakes would be a fundamental dif-ference of the MPES with the YLES where the burst of migrations are made of multiplets triggered by each step of dike intrusion.

7. Concluding remarks

The Basin and Range Province background extensional stress regime is considered the dominant stress field associated with the Mw7.3 in 1959 on the Hebgen Lake fault. We suggest that the same background stress triggered the Yellowstone multiplet activity, preferentially in the aftershock area of the 1959 Hebgen Lake earthquake and western Yellowstone. The most active faults in Yellowstone, shown by multiplets, are in the Hebgen area, including the Gallatin Range and in the southwestern Gallatin-Mt. Wasburn fault zone (Fig. 1). The stress accumulation along Yellowstone's main faults tends to produce a uniform stress field, before the triggering of a tectonic swarm on optimally oriented faults, which takes the cycle back to a slightly heterogeneous background stress field.

Tectonic and magmatic swarms involve two different types of rupture mechanisms that are characterized by multiplet evolution. Tectonic swarms are characterized by multiplets with aftershocks and daily to weekly durations. Tectonic swarms can involve hydrothermal fluid migration, such as we have shown for the autumn 1985 northwest Yellowstone caldera earthquake swarm, and maintain their multiplet properties during a slow migrating phase. Swarms with complete stepwise migration, bursts of multiplets with hourly to daily durations and lacking multiplet main-shocks can be triggered by magma intrusion, like in the 2008–2009 Yellowstone Lake earthquake swarm. Thermo-dynamical modeling of multiplets shows that for the Yellowstone Lake earthquake swarm, the migrating swarm front and surface extension could be produced by the injection of 5 m^3 of rhyolitic magma per second in a 9 to 13 cm thick dike. The fact that this model does work for the Yellowstone Lake earthquake swarm does not argue against other processes, and some other modeling experiences would certainly produce interesting new constraints.

We thus suggest that the stress accumulation between individual swarms activates two different kinds of seismogenic structures depending on the stress state of the Yellowstone magma system. During a crustal subsidence phase, pre-existing structures are preferentially re-activated resulting in a clustering rate increase. During an uplift phase, the activity of single seismic sources abnormally increases involving neo-faulting or the rupture of rarely solicited and healed faults. This last type of tectono-magmatic activity is likely prevalent throughout the Yellowstone caldera and our new broadband seismic instrumentation will provide key data for future research.

Acknowledgments

References

Baraldo, A., Rinaldi, C.A., 2000. Stratigraphy and structure of Deception Island, South Shetland Islands, Antarctica. Journal of South American Earth Sciences 13 (8), 785–796.

Benoit, J.P., McNutt, S.R., 1996. Global volcanic earthquake swarm database and preliminary analysis of volcanic earthquake swarm duration. Annali di Geofisica XXXIX (2).

Bergman, E.A., Solomon, S.C., 1990. Earthquake swarms on the Mid-Atlantic Ridge: products of magmatism or extensional tectonics? Journal of Geophysical Research 95 (B4), 4943–4965.

Bottinga, Y., Weill, D.F., 1970. Densities of liquid silicate systems calculated from partial molar volumes of oxide components. American Journal of Science 269 (2), 169–182.

Brancato, A., Gresta, S., 2003. High precision relocation of micro-earthquakes at Mt. Etna (1991–1993 eruption onset): a tool for better understanding the volcano seismicity. Journal of Volcanology and Geothermal Research 124 (3–4), 219–239.

Carmona, E., Almendros, J., Pena, J., Ibanez, J., 2010. Characterization of fracture systems using precise array locations of earthquake multiplets: an example at deception Island volcano, Antarctica. Journal of Geophysical Research 115 (B6), B06,309.

Chang, W.-L., Smith, R.B., 2002. Integrated seismic-hazard analysis of the Wasatch Front, Utah. Bulletin of the Seismological Society of America 92 (5), 1904–1922.

Chang, W.-L., Smith, R.B., Wicks, C., Farrell, J.M., Puskas, C.M., 2007. Accelerated uplift and magmatic intrusion of the Yellowstone Caldera, 2004 to 2006. Science 318 (952).

Chang, W.L., Smith, R.B., Farrell, J., Puskas, C.M., 2010. An extraordinary episode of Yellowstone caldera uplift, 2004–2010, from GPS and InSAR observations. Geophysical Research Letters 37 (23), L23302.

Christiansen, R., 2001. The Quaternary and Pliocene Yellowstone Plateau volcanic field of Wyoming, Idaho, and Montana. U.S. Geological Survey Professional Paper 729-G.

Christiansen, R.L., Lowenstern, J.B., Smith, R.B., Heasler, H., Morgan, L.A., Nathenson, M., Mastin, L.G., Muffler, L.J.P., Robinson, J.E., 2007. Preliminary assessment of volcanic and hydrothermal hazards in Yellowstone National Park and vicinity. U.S. Geological Survey Open-File Report, 1071.

DeNosaquo, K.R., Smith, R.B., Lowry, A.R., 2009. Density and lithospheric strength models of the Yellowstone-Snake River Plain volcanic system from gravity and heat flow data. Journal of Volcanology and Geothermal Research 188 (1–3), 108–127.

Everitt, B.S., 1974. Cluster Analysis. Heinemann Educational for Social Science Research Council, London.

Evison, F.F., Rhoades, D.A., 1998. Long-term seismogenic process for major earthquakes in subduction zones. Physics of the Earth and Planetary Interiors 108 (3), 185–199.

Farrell, J.M., 2007. Space–time seismicity and development of a geographical information system database with interactive graphics for the Yellowstone region. Master's thesis, Department of Geology and Geophysics, University of Utah.

Farrell, J.M., Husen, S., Smith, R.B., 2009. Earthquake swarm and b-value characterization of the Yellowstone volcano-tectonic system. Journal of Volcanology and Geothermal Research 188 (1–3), 260–276.

Farrell, J.M., Smith, R.B., Taira, T., Chang, W.L., Puskas, C.M., 2010a. Dynamics of the intense 2008–2009 Yellowstone Lake earthquake swarm. Geophysical Research Letters 37, L19305.

Farrell, J., Puskas, C., Smith, R.B., 2010b. Large earthquake swarms of the Yellowstone volcanic system. Biennial UNAVCO Science Meeting, Boulder, Colorado.

Feng, L., Newman, A., 2009. Constraints on continued episodic inflation at long Valley caldera, based on seismic and geodetic observations. Journal of Geophysical Research 114.

Fournier, R.O., 1999. Hydrothermal processes related to movement of fluid from plastic into brittle rock in the magmatic-epithermal environment. Economic Geology 94 (8), 1193–1211.

Fremont, M.J., Malone, S.D., 1987. High precision location of earthquakes at Mount St Helens, Washington. Journal of Geophysical Research 92 (B10), 10,223–10,236.

Geller, R.J., Mueller, C.S., 1980. Four similar earthquakes in central California. Geophysical Research Letters 7 (10), 821–824.

Got, J.-L., Okubo, P., 2003. New insights into Kilauea's volcano dynamics brought by large-scale relative relocation of microearthquakes. Journal of Geophysical Research 108 (B7), 2337.

Got, J.-L., Fréchet, J., Klein, F.W., 1994. Deep fault plane geometry inferred from multiplet relative relocation beneath the south flank of Kilauea. Journal of Geophysical Research 99 (B8), 15,375–15,386.

Hansen, S., Schwartz, S., DeShon, H., Gonzalez, V., 2006. Earthquake relocation and focal mechanism determination using waveform cross correlation, Nicoya Peninsula, Costa Rica. Bulletin of the Seismological Society of America 96 (3), 1003–1011.

Hill, D., 1977. A model for earthquake swarms. Journal of Geophysical Research 82, 1347–1352.

Hill, D., Langbein, J., Perigean, S., 2003. Relations between seismicity and deformation during unrest in long valley caldera, California, from 1995 through 1999. Journal of Volcanology and Geothermal Research 127 (3–4), 175–193.

Holtkamp, S.G., Brudzinski, M.R., 2011. Earthquake swarms in circum-Pacific subduction zones. Earth and Planetary Science Letters 305 (2), 215–225.

Holtkamp, S., Pritchard, M., Lohman, R., 2011. Earthquake swarms in South America. Geophysical Journal International 187 (1), 128–146.

Husen, S., Taylor, R., Smith, R.B., Healser, H., 2004a. Changes in geyser eruption behavior and remotely triggered seismicity in Yellowstone National Park produced by the 2002 M 7.9 Denali fault earthquake, Alaska. Geology 32 (6), 537.

Husen, S., Smith, R.B., Waite, G.P., 2004b. Evidence for gas and magmatic sources beneath the Yellowstone volcanic field from seismic tomographic imaging. Journal of Volcanology and Geothermal Research 131 (3–4), 397–410.

Imoto, M., Kishimoto, Y., 1977. Statistical search for migrations of aftershock sequences. Bulletin of the Disaster Prevision Institute, Kyoto University 27-3 (249).

Martini, F., Bean, C., Saccorotti, G., Viveiros, F., Wallenstein, N., 2009. Seasonal cycles of seismic velocity variations detected using coda wave interferometry at Fogo volcano, São Miguel, Azores, during 2003-2004. Journal of Volcanology and Geothermal Research 181 (3–4), 231–246.

Massin, F., Ferrazzini, V., Bachelery, P., Nercessian, A., Duputel, Z., Stauncher, T., 2011. Structures and evolution of the plumbing system of Piton de la Fournaise volcano inferred from clustering of 2007 eruptive cycle seismicity. Journal of Volcanology and Geothermal Research 202 (1–2), 96–106.

McNally, K.C., Kanamori, H., Pechmann, J.C., Fuis, G., 1978. Earthquake swarm along the San Andreas Fault near Palmdale, Southern California, 1976 to 1977. Science 201 (4358), 814–817.

Mogi, K., 1963. Some discussions on aftershocks, foreshocks and earthquake swarms: the fracture of a semi-infinite body caused by an inner stress origin and its relation to the earthquake phenomena (third paper). Bulletin of the Earthquake Research Institute 41, 615–658.

Morgan, P., Blackwell, D.D., Spafford, R.E., Smith, R.B., 1977. Heat flow measurements in Yellowstone Lake and the thermal structure of the Yellowstone Caldera. Journal of Geophysical Research 82 (26), 3719–3732.

Obrebski, M., Allen, R.M., Xue, M., Hung, S.H., 2010. Slab-plume interaction beneath the Pacific Northwest. Geophysical Research Letters 37, L14305.

Pickering-White, B.J., Smith, R.B., Husen, S., Farrell, J.M., Wong, I., 2009. Seismicity and earthquake hazard analysis of the Teton-Yellowstone region. Journal of Volcanology and Geothermal Research 188 (277–296), 26–56.

Poupinet, G., Ellsworth, W.L., Fréchet, J., 1984. Monitoring velocity variations in the crust using earthquake doublets: an application to the Calaveras fault, California. Journal of Geophysical Research 89 (B7), 5719–5731.

Puskas, C., Smith, R.B., Meertens, C.M., Chang, W.L., 2007. Crustal deformation of the Yellowstone–Snake River Plain volcano-tectonic system: Campaign and continuous GPS observations, 1987–2004. Journal of Geophysical Research 112, B03401.

Puskas, C., Hodgkinson, K., Farrell, J., Chang, W.L., Massin, F., 2012. A comparison of deformation and seismicity at the Yellowstone Caldera during the 2004–2010 uplift episode. Seismological Society of America Annual Meeting.

Reches, Z., Fink, J., 1988. The mechanism of intrusion of the Inyo dike, Long Valley caldera, California. Journal of Geophysical Research 93 (B5), 4321–4334.

Roman, D., Cashman, K., 2006. The origin of volcano-tectonic earthquake swarms. Geology 34 (6), 457–460.

Rowe, C., Aster, R., Borchers, B., Young, C., 2002. An automatic, adaptive algorithm for refining phase picks in large seismic data sets. Bulletin of the Seismological Society of America 92, 1660–1674.

Rowe, C., Thurber, C., White, R., 2004. Dome growth behavior at Soufriere Hills Volcano, Montserrat, revealed by relocation of volcanic event swarms, 1995–1996. Journal of Volcanology and Geothermal Research 134, 199–221.

Rubin, A.M., 1992. Dike-induced faulting and graben subsidence in volcanic rift zones. Journal of Geophysical Research 97 (B2), 1839–1858.

Rubin, A.M., 1995. Propagation of magma-filled cracks. Annual Review of Earth and Planetary Sciences 23 (1), 287–336.

Rubin, A.M., Gillard, D., Got, J., 1999. Streaks of microearthquakes along creeping faults. Nature 400 (6745), 635–641.

Ruppert, N.A., Prejean, S., Hansen, R.A., 2011. Seismic swarm associated with the 2008 eruption of Kasatochi Volcano, Alaska: Earthquake locations and source parameters. Journal of Geophysical Research 116, B00B07.

Seebeck, H., Nicol, A., 2009. Dike intrusion and displacement accumulation at the intersection of the Okataina Volcanic Centre and Paeroa Fault zone, Taupo Rift, New Zealand. Tectonophysics 475, 575–585.

Shane, P., Martin, S.B., Smith, V.C., Beggs, K.F., Darragh, M.B., Cole, J.W., Nairn, I.A., 2007. Multiple rhyolite magmas and basalt injection in the 17.7 ka Rerewhakaaitu eruption episode from Tarawera volcanic complex, New Zealand. Journal of Volcanology and Geothermal Research 164 (1–2), 1–26.

Shelly, D.R., et al., 2012. Dynamics of migrating earthquake swarms at Yellowstone and Mount Rainier Evidence for fluid triggering? SCEC Annual Meeting.

Smith, R.B., Jordan, M., Steinberger, B., Puskas, C.M., Farrell, J.M., Waite, G.P., Husen, S., Chang, W.L., O'Connell, R., 2009. Geodynamics of the Yellowstone hotspot and mantle plume: seismic and GPS imaging, kinematics, and mantle flow. Journal of Volcanology and Geothermal Research 188 (1–3), 26–56.

Sykes, L.R., 1970. Earthquake swarms and sea-floor spreading. Journal of Geophysical Research 75 (32), 6598–6611.

Taisne, B., Tait, S., 2011. The effect of solidification on propagating dike. Journal of Geophysical Research 116 (B1), B01206.

Thelen, W., Crosson, R., Creager, K., 2008. Absolute and relative locations of earthquakes at Mount St. Helens, Washington, using continuous data: implications for magmatic processes. In: Sherrod, D.R., Scott, W.E., Stauffer, P.H. (Eds.), A volcano rekindled: the renewed eruption of Mount St. Helens, 2004–2006: U.S. Geological Survey Professional Paper, 1750, pp. 71–95.

Ukase, M., Tsukahara, H., 1996. Earthquake swarms and dike intrusions off the east coast of Izu Peninsula, central Japan. Tectonophysics 253, 285–303.

Waite, G.P., Smith, R.B., 2002. Seismic evidence for fluid migration accompanying subsidence of the Yellowstone caldera. Journal of Geophysical Research 107 (B9), 2177.

Waite, G.P., Smith, R.B., 2004. Seismotectonics and stress field of the Yellowstone volcanic plateau from earthquake first-motions and other indicators. Journal of Geophysical Research 109 (B02301).

Waite, G.P., Smith, R.B., Allen, R.M., 2006. Vp and Vs structure of the Yellowstone hot spot from teleseismic tomography: evidence for an upper mantle plume. Journal of Geophysical Research 111, B04303.

Waldhauser, F., Ellsworth, W., 2000. A double-difference earthquake location algorithm: method and application to the Northern Hayward Fault, California. Bulletin of the Seismological Society of America 90 (6), 1353–1368.

Waldhauser, F., Schaff, D., 2008. Large-scale relocation of two decades of northern California seismicity using cross-correlation and double-difference methods. Journal of Geophysical Research 113 (5), 2736.